

Highly efficient natural dye-sensitized photoelectrochemical solar cells based on Cu-doped zinc oxide thin film electrodes

M. D. Tyona^{a*}, R. U. Osuji^b, F. I. Ezema^b, S. B. Jambure^c and C. D. Lokhande^c

^aDepartment of Physics, Benue State University, Makurdi, Nigeria

^bDepartment of Physics and Astronomy, University of Nigeria, Nsukka, Nigeria

^cDepartment of Physics, Shivaji University, Kolhapur, (M.S.) India

ABSTRACT

The current work under studied the photosensitizing action of a natural dye obtained from *Indigofera arrecta* plant (a herbicacious plant) on nanocrystalline Cu-doped zinc oxide (CZO) thin film electrodes synthesized by chemical bath deposition (CBD) technique. This dye, having strong absorption in the visible range with almost constant absorption peak, was found to convert visible light in the range of 300–750 nm into electrical energy. The electron injection by photo-excited dye molecules into the conduction band of CZO was evidenced by electrochemical impedance lowering of the dye-capped CZO electrode at optimum Cu impurity level of 3 at.% which facilitates fast charge carrier transport in the semiconductor. On irradiation of the dye-capped CZO thin film electrodes with white light of intensity 80 mW/cm², power conversion efficiency (η) of the (CZO electrode/*Indigofera arrecta* plant dye-containing electrolyte/platinum electrode) cell was found to be 4.16 % with fill factor of 0.54. The values of short circuit photocurrent I_{sc} , and open-circuit photovoltage V_{oc} , measured to be 6.8 mA/cm² and 0.91 V show the applicability of the natural dye in solar cells.

Keywords: Photoelectrochemical cell, *Indigofera arrecta* plant dye, Dye-sensitized solar cell, Cu-doped ZnO, Photoelectrode, Thin films

INTRODUCTION

Dye-sensitized Photoelectrochemical solar cells (PECs) have attracted the attention of many researchers in this area due to its high potentials as cost-effective, efficient and an environmentally friendly alternative to solid photovoltaic devices [1, 2]. The overwhelming success of Grätzel and co-workers in achieving a significantly high light-to-electrical conversion efficiency (as high 11%) with a dye sensitized solar cell(DSSC)using nanocrystalline TiO₂thin film electrode sensitized with RuII(2,20-bipyridle-4,40-dicorboxylate)2 (NCS)₂[1, 3],arose the curiosity of many researchers to explore different kinds of dyes [4-7].

In dye-sensitized solar cells (DSSCs), semiconductor electrode is the major component. The choice of a suitable semiconductor material and appropriate synthetic method will produce thin films of the material with effective surface area and porosity which will greatly enhanced its DSSC performance [1, 4, 9]. Such films facilitate greater adsorption of dye molecules on their surfaces, which will improve the absorption of incident light and enhances power conversion efficiency [1, 4, 9]. TiO₂ semiconductor has been extensively studied for its application in DSSCs than ZnO semiconductor. However, ZnO possessed similar properties as TiO₂ and furthermore, ZnO has higher electron mobility than TiO₂ and so could be an even better material for DSSCs than TiO₂ [14].

Since wide band gap semiconductors with energy band gap $E_g > 3$ eV are the most stable materials for PEC solar cells, this limits their light absorption only below a threshold wavelength λ_g [1, 14]. ZnO semiconductor with energy band gap of about 3.37 eV can only absorb within the ultraviolet region of the solar spectrum. Therefore it is imperative to reduce the band gap of ZnO in order to extend its absorption towards the longer wavelengths. It has been reported that Cu-doping can successfully narrow the bandgap of ZnO and extend the photoresponse in the long-wavelength region [1, 4, 9].

In the history of dye-sensitization of photoelectrodes in DSSCs, ruthenium based dyes have been the most widely researched and the best performing dyes in combination with nanocrystalline semiconductor (ZnO or TiO_2) [8-11]. Such cells have also shown remarkable photochemical stability on long-term operation. However, one of the important factors in the choice of dyes is the cost. Because Ru is a rare metal with very low annual yield, metal-free-organic dyes have been desired and a wide variety of pure organic dyes have been investigated for application in DSSCs [12, 13]. These include: coumarin, metalloporphyrin, ferrocene, indoline, hemicyanine, Rose Bengal and rhodamine 6G among others [3, 7, 15-17]. In the current search for newer dyes for DSSC applications, plant dyes are being discovered as efficient sensitizers. Many organic sensitizers including plant dye has been investigated; Souad et al. [12] reported aI_{sc} of 0.93 mAcm^{-2} , V_{oc} of 394 mV and a conversion efficiency, η of 1.5 % for Sumac (a flowering plant). Roy et al. [18] also reported DSSC performance of Rose Bengal dye as sensitizer with I_{sc} and V_{oc} of 3.22 mAcm^{-2} and 0.89 V, respectively resulting to η of 2.09 %. Hara et al. [19] reported aI_{sc} of 14.0 mAcm^{-2} , V_{oc} of 0.60 V, a η of 6.0 % and ff of 0.71 for coumarin dye on nanocrystalline TiO_2 , the highest performance among DSSCs based on organic-dye as photosensitizers.

Organic dyes, especially natural dyes (from plants) can replace synthetic dyes since they can be easily extracted from fruits, vegetable and flowers with simple and direct chemical procedures, whereas the former normally requires many steps procedures, organic solvents and purification procedures [20-23]. The pigments are present in the different part of the plant including flowers petals, fruits, leaves, stems and roots.

A natural dye extracted from *Indigofera arrecta* (Beba, a herbicidal plant from the Guinea savannah region of Benue State, Nigeria) is extensively used for dyeing locally woven textile materials. This dye has never been investigated for its chemical structure and DSSC applications however; it shows high potential as an efficient photosensitizer in DSSCs. The current work investigates the DSSC performance of a natural dye extracted from *indigofera arrecta* plant as sensitizers of nanocrystalline Cu-doped ZnO (CZO) thin film electrodes in acetonitrile [24].

MATERIALS AND METHODS

2.1. Materials

$\text{Zn}(\text{NO}_3)_2 \cdot 6\text{H}_2\text{O}$ (sd fine chemicals) was used as the source of Zn^{2+} , $(\text{CuCl}_2 \cdot 2\text{H}_2\text{O})$ (Chemcofine-India) as the source of Cu^{2+} and NH_3 solution (28 %) (Thomas Baker) was the complexing agent. KI (Romaali-India) and I (Lobachemie) dissolved in acetonitrile (SDFCL-India) was used as electrolyte and redox agent, respectively. Fresh leaves of *indigofera arrecta* plant were obtained from its growth environment, dried and crushed into fine powder. All chemicals were used as received, without any further purification.

2.2. Methods

CZO thin films were synthesized by chemical bath deposition technique. An aqueous solution of 0.1 M $\text{Zn}(\text{NO}_3)_2 \cdot 6\text{H}_2\text{O}$ was prepared, to this solution, cupric chloride ($\text{CuCl}_2 \cdot 2\text{H}_2\text{O}$) was added. Cu content in the solution was varied from 1 to 5 at. %. Aqueous NH_3 solution (28 %) was then added under constant stirring at room temperature. A greenish white precipitate of $\text{Cu-Zn}(\text{OH})_2$ was initially observed, which subsequently dissolved back into the solution upon further addition of NH_3 solution. The solution was maintained at $\text{pH} \approx 11.5$. Ultrasonically cleaned microscope glass slide and stainless steel substrates were immersed vertically in the solution using a bakelite holder and the bath temperature was maintained at 353 K. The substrates coated with CZO thin film were removed after 5 h, washed with double distilled water dried in air and preserved in the vacuum desiccator. Further, as-deposited films were air annealed at 673 K for 2 h.

Fresh leaves of *indigofera arrecta* plant were dried in an airy room shielded from direct sun rays until they were completely dried. The dried leaves were crushed into fine powder and an appropriate quantity was heated in a beaker containing acetonitrile at a temperature of 313 K for 5 h and then filtered using WHATMAN filter paper to obtain a

fine greenish dye solution. The CZO thin film electrodes were immersed in the dye solution for about 12 h to fix the dye onto their surfaces. After dye adsorption, the colour of the films were changed to dark green. The electrodes were rinsed in double distilled water to remove the loosely adsorbed dye molecules and finally dried in air for use. The dye was characterized for optical absorption.

2.3. Apparatus and instruments

Unless otherwise stated, all DSSC measurements were carried out in a two-electrode, single compartment cell. A platinum wire was used as a counter electrode and the *indigofera arrecta* dye-sensitized CZO electrode was used as the photoelectrode.

A potentiostat was used for all current-potential measurements. For DSSC measurements, 80W xenon arc lamp was used as the source of white light to illuminate the semiconductor photoelectrode area of 1 cm². The absorption spectrum of the dye in acetonitrile solution was recorded on a Shimadzu, UV-1800 spectrophotometer. Structural properties of the CZO thin films were studied using Philips PW 1830 X-ray diffractometer with CuK α radiation ($\lambda = 1.5406 \text{ \AA}$) in the range $20 - 80^\circ$ in 2θ . Surface morphology was studied with the scanning electron microscope (SEM) (using JOEL JSM-6360). The surface wettability of the films was studied using water contact angle meter.

RESULTS AND DISCUSSION

3.1. Structural characterizations of CZO thin films

X-ray diffraction technique is used for the determination of crystal structure and lattice parameters along with structural changes and identification of phases of the prepared CZO thin films. Fig. 1 depicts the XRD patterns of undoped ZnO and CZO thin films annealed at 673 K. It was observed that all the film samples were polycrystalline with hexagonal wurtzite structure with lattice constants $a=3.24982 \text{ \AA}$ and $c=5.20661 \text{ \AA}$ corresponding to those of the ZnO patterns from the JCPDS data card (Powder Diffraction File, Card no: 00-036-1451). From the XRD patterns, a strong preferential growth of high intensity in the (002) crystal plane was observed for the undoped ZnO and CZO films with 3 at. % Cu concentration, which is the most dense plane in wurtzite ZnO, however, for 1 and 5 at. % Cu concentrations, it was highly diminished [25, 26].

The observed decrease in intensity of the ZnO peak upon incorporation of Cu impurities (ie; Cu/Zn of 1 at %) could be due to fact that the incorporation of Cu impurities into the ZnO lattice induces some crystallographic defects and hence reduced the crystalline quality of the film [27-29]. By increasing the Cu content to 3 at. % (optimum concentration), the carrier concentration and mobility in the conduction band of the semiconductor also increases [30, 31] thereby reducing the amount of crystallographic defects in the film [32]. This result suggests that the crystallinity of the film in the ZnO (002) plane at this concentration of Cu would improve significantly as depicted in Fig. 1c [32]. As the doping concentration was further increased to 5 at. %, the crystalline quality of the film sample decreased significantly. This is an indication that there is more compressive strain in the films at higher doping level [33, 34]. Additionally, according to Barna and Adamik structure zone model for polycrystalline metallic films [33], as the impurities content increased, more impurities segregation occurred at the grain boundaries of the film which result in shrinkage in grains size [33] which is similar to the case observed here.

A shift in angular peak positions in (2θ) corresponding to the (002) plane in ZnO upon incorporation of Cu impurities was observed. It was clearly noticed that a diffraction peak shift of 0.545° in 2θ towards the higher angle occurred for all CZO films. This could be assigned to the difference in ionic radii of Zn²⁺ and Cu²⁺ (which is higher for Zn²⁺ as compared to Cu²⁺) such that the length of the c-axis is expected to be shorter when Cu atoms are substituted into Zn sites in the crystal lattice [25, 32-34]. According to Shannon [34], the 4-fold coordinated Zn²⁺ and Cu²⁺ cations have ionic radii of 0.074 and 0.057 nm, respectively and stable electronic configurations: Zn²⁺(3d¹⁰) and Cu²⁺(3d⁹). The 4-fold coordinated, Cu¹⁺ has ionic radius of 0.06 nm Cu¹⁺(3d¹⁰) [34].

The mean crystallite size of the CZO thin films along the plane of most preferred growth (002) was calculated on the basis of full width at half maxima (FWHM) using Scherrer's formula [30]:

$$D = \frac{0.9\lambda}{\beta \cos \theta} \quad (2)$$

where λ , β , and θ are the X-ray wavelength ($\lambda = 1.54056 \text{ \AA}$), fullwidth at half maximum (FWHM) and diffraction peak angle, respectively. The estimated crystallite sizes showed that the mean crystallite size of undoped ZnO film increased from 28 to 30 nm for CZO as depicted in Table 1.

Table 1. Estimated crystallite sizes of CZO thin films using (002) crystal plane

% Doping of Cu	Mean crystallite size (nm)
0	28
1	7
3	30
5	8

3.2. Surface characterizations of CZO thin films

The surface morphology of CZO thin films was studied using scanning electron microscope (SEM) images (JOEL JSM-6360). In chemical bath deposition of ZnO thin film, as-deposited films contained hydroxide and other impurities [35], so thermal annealing was necessary. Thermal annealing causes remarkable change in the surface morphology of the thin films [36]. Fig. 2 depicts SEM micrographs of the CZO thin films (as-deposited and annealed) with different Cu concentrations (0, 1, 3 and 5 at %). These SEM micrographs confirmed that the surface morphology of the films was affected by the concentration of the dopant. The grain size of the films decreases upon introduction of the Cu impurities as suggested by XRD study. This behaviour could also be assigned to the difference in the ionic radii of Zn and the doping element, Cu [25, 37]. Further, with increasing Cu concentration (up to an optimum concentration of 3 at %), the microstructures of the film became denser as in Fig. 2f.

The scanning electron micrograph of the undoped ZnO thin films, both as-deposited and annealed showed fibrous nanorods of approximately 115 nm as in Fig. 2(a and b). For the CZO, the as-deposited (ie; 1 at %) film as depicted in Fig. 2 (c), showed fibrous surface morphology with well-defined nanodendritic rods grown randomly on the substrate as thin solid films of Cu-Zn(OH)₂. Each dendritic rod is crystalline and indexed to hexagonal crystal structure, as seen in Fig. 2 (c). The average thickness of the rods was of the order of ≈ 40 nm. After annealing at 673 K, the hydroxide phase in the nanodendritic rods was converted to pure CZO with fibrous nanorods morphology of average rod diameter of ≈ 30 nm and randomly oriented, leading to large surface area as depicted in Fig. 2 (d). Such novel morphology may find applications in photoelectrochemical (PEC) solar cells, gas sensors and super capacitors [38].

Fig. 2 (e and f) represents the SEM micrographs of as-deposited and annealed CZO with Cu:Zn of 3 at. %. The as-deposited film samples are identified with dense and vertically aligned nanorods morphology of varying rod sizes with average rod diameter of 120 nm and high porosity as well as high surface roughness. Post annealing treatment at 673 K, converted the former morphology to fibrous nanorods, vertically aligned with well-defined and nearly uniform rod sizes (mean rod diameter of ≈ 112 nm) as depicted in Fig. 2 (f). This morphology is suitable for DSSCs application (Fig. 2 g and h shows cross-sectional view of the nanorods in f).

The SEM micrographs of CZO with Cu concentration of 5 at. % are depicted in Fig. 2 (i) and (j). As-deposited film samples, (i), show densely oriented nanodendrites. After post annealing treatment at 673 K, dense, uniformly oriented nanodendrites with fine structures were obtained as in (j). These observations agree with that observed by Chow et al. [25] using chemical synthesis of CZO thin films, and is suitable for PEC solar cell application.

3.3. Characterization for surface wettability of CZO

Wettability involves the interaction between liquid and solid in contact. The wetting behaviour of thin film is characterized by the value of contact angle, a microscopic parameter. The contact angle is an important parameter in surface science and its measurement provides a simple and reliable technique for the interpretation of surface energies. Both super-hydrophilic and super-hydrophobic surfaces are important for practical applications [39].

PEC solar cell application of CZO thin film requires a film of high porosity with high surface roughness which implies hydrophilic or super-hydrophilic surface. Contact angle provides information relating to the state of hydrophilicity of a thin film. In the present case, Fig. 3 depicts the measured water contact angles of the CZO thin films which indicated that all the films are hydrophilic. This result implies that the porosity of the film increases upon thermal annealing at 673 K which means larger surface area and better dye adsorption as earlier asserted; resulting in enhanced photo absorption.

It was also observed that the water contact angles decreased (as compared with undoped sample Fig. 3a and b) upon incorporation of Cu impurities up to optimal percentage impurity of 3 at. % (Fig. 3e and f) and further increases as the impurity concentration is increased beyond this level (Fig. 3g and h). This result is in agreement with the earlier observations from SEM. Since the morphology is porous (pores of the size of few microns), the water goes in to the pores and crevices making contact angle hydrophilic. The hydrophilic nature of the film has been attributed to the fibrous morphology of the films [40].

3.4. Optical property of *indigofera arrecta* plant dye

The absorption spectra of *indigofera arrecta* plant dye extracted in acetonitrile is shown in Fig. 4 along with that of unsensitized CZO thin film for comparison (only 3 at. %). It is clear that the dye has shown very good light absorption across the spectrum from UV to visible light in the range of 300-750 nm wavelengths with almost constant absorption peak across the range. Hence *indigofera arrecta* plant dye, having absorbs light effectively across the visible spectrum can be used as photosensitizer for wide-band gap semiconductors, such as CZO ($E_g = 3.14$ eV), which alone cannot absorb reasonably in the visible light spectrum as shown in Fig. 4.

Photoelectrochemical studies

4.1. Current-potential (I-V) curves

Photoelectrochemical characteristic of an electrode/electrolyte interface is one of the important tools in identifying stability of a semiconductor material (electrode) for electrochemical photovoltaic applications [41]. To investigate photoelectrochemical activities of the synthesized CZO thin films in the present work, all experiments were performed in a single compartment cell in polyiodide solution as the electrolyte. Photoelectrode (CZO thin film) area of 1 cm^2 was illuminated with an input power (P_{in}) of 80 mW/cm^2 from a xenon arc lamp. Fig. 5 depicts I-V curves of CZO PEC solar cells with different Cu concentration (1, 3 and 5 at. %), sensitized by *indigofera arrecta* plant dye. A careful perusal of these curves shows that in the dark, the current obtained at each CZO electrode was not zero however very low. This could be due to the fact that the cell might be partially illuminated by the background light in the experimental room. Further, when the electrodes were illuminated with white light, all photoelectrodes showed significantly high photocurrents though; higher photocurrent was recorded for the CZO sample with Cu:Zn of 3 at. %. These currents were comparatively higher than that recorded for undoped ZnO sample (as shown in the inset of Fig. 5a, 0.29 mA/cm^2) under the same conditions; this confirmed that CZO semiconductor materials are better candidates for PEC cell application [44].

This improvement in photocurrent of the electrodes upon dye-sensitization can be assigned exclusively to charge carriers injection by photoexcited dye molecules alongside the valence electrons excited by the white light which increases total charge carriers and hence higher photocurrent as observed [24]. This is a normal phenomenon because white light consists of photons of energy $h\nu \geq E_g$ of ZnO that can excite the electrons from the valence band to conduction band of the semiconductor to produce photocurrent [19, 24].

It was observed here that the photocurrent increased with Cu concentration with the highest current recorded for Cu:Zn of 3 at. %. Further increase in Cu concentration beyond 3 at. %, current decreased rapidly; thus confirming the earlier assertion that 3 at. % Cu concentration is the optimum doping level for CZO for DSSC applications. This enhanced performance at optimal doping concentration is probably due to optimal carrier concentration reached in the semiconductor which facilitates fast electron transport and consequent suppression of charge recombination activities [45].

The reason why *indigofera arrecta* plant dye can effectively sensitize CZO is due to their energy band gaps [24] (1.91 eV estimated for *indigofera* and 2.96, 3.14 and 2.7 eV for CZO with Cu:Zn of 1, 3 and 5 at. %). When *indigofera arrecta* dye molecules absorb photons with energies greater than 1.91 eV, the electrons in the excited states of *indigofera arrecta* plant dye can be quickly injected into the conduction bands of CZO nanostructures [1, 22]. This attests to the improved performance of *indigofera arrecta* plant dye on nanocrystalline CZO electrodes. The estimated photocurrent and photovoltage values are presented in Table 2.

Table 2. PEC solar cell parameters of CZO thin film electrodes sensitized by *indigofera arrecta* plant dye

CZO Electrodes with Cu at %	Photocurrent (I_{sc}) [mA/cm ²]	Photovoltage (V_{oc}) [mV]	I_{max} (mA/cm ²)	V_{max} (mV)
0	0.29	595.0	0.18	421.0
1	0.91	656.0	0.60	535.0
3	6.80	844.0	4.10	742.0
5	1.20	790.0	0.59	667.0

Table 3. Equivalent electrical circuit analog data estimated from the electrochemical cell measurement of *indigofera arrecta* plant dye-sensitized CZO (with different Cu dopings) PEC solar cell measured in dark condition in a 2-electrode configuration at bias potential of 0.656, 0.914 and 0.790 V (a) 1 at % (b) 3 at % and (c) 5 at %

(a)

Parameter	Value	Error
Qy1	3.26E-11	1.42E-10
Qa1	1.606764	0.352781
R1	2089.592	5801.134
R2	33.87533	22.39476
Qy2	0.00017	0.000253

(b)

Parameter	Value	Error
C1	7.84E-08	5.68E-08
R1	51.88532	15.10799
C2	0.00021	0.000858
R2	76.55203	310.4269
W	0.000986	0.001167

(c)

Parameter	Value	Error
Qy1	3.88E-10	1.76E-09
Qa1	1.410639	0.370123
R1	340852.8	4.81E+08
R2	45.23995	26.84146
Qy2	0.000402	0.001006
Qa2	0.502641	0.308693

Table 4. Estimated values of power conversion efficiencies and fill factors of *indigofera arrecta* plant dye-sensitized CZO PEC solar cells

CZO Electrodes with % Cu	Efficiency (%)	Fill Factor (FF)
0	0.10	0.44
1	0.40	0.54
3	4.16	0.54
5	0.49	0.42

4.2. Electrochemical impedance spectroscopy (EIS) study

Electrochemical Impedance Spectroscopy (EIS) is a semi quantitative technique and is versatile for investigating the dynamics of the bound or mobile charges in the bulk or interfacial region of a PEC solar cell system [46]. In EIS measurements, the potential applied to the solar cell is perturbed by a small amplitude sinusoidal modulation and the resulting sinusoidal current response is measured as a function of the modulation frequency system. It is one of the most useful experimental techniques, as it permits a simultaneous characterization of the different processes taking place in the cell; that is, at the semiconductor, in the electrolyte and at the counter-electrode side [47]. The electrical current response is measured when a certain sinusoidal voltage is applied to the system. This current response will be a sinusoid at the same frequency, but shifted in phase [47].

EIS of CZO electrode annealed at 673 K was carried out using a Frequency Response Analyzer coupled to a Potentiostat in a two-electrode mode [46,47]. The electrochemical processes occurring in the entire cell arrangement were evaluated in the dark condition. The EIS data are commonly analyzed by fitting into an equivalent electrical circuit model [48]. Most of the circuit elements in the model are common electrical elements such as resistors, inductors and capacitors. The impedance response of such ideal resistors, inductors and capacitors are given below [46]:

$$Z_R = R \quad (3)$$

$$Z_L = j\omega L \quad (4)$$

$$Z_C = \frac{1}{j\omega C} \quad (5)$$

EIS models usually consist of a number of elements connected in the network either in series and/or parallel combinations. For a highly nested electrical circuit, the equivalent impedance is calculated by lumping together the simple circuits [49].

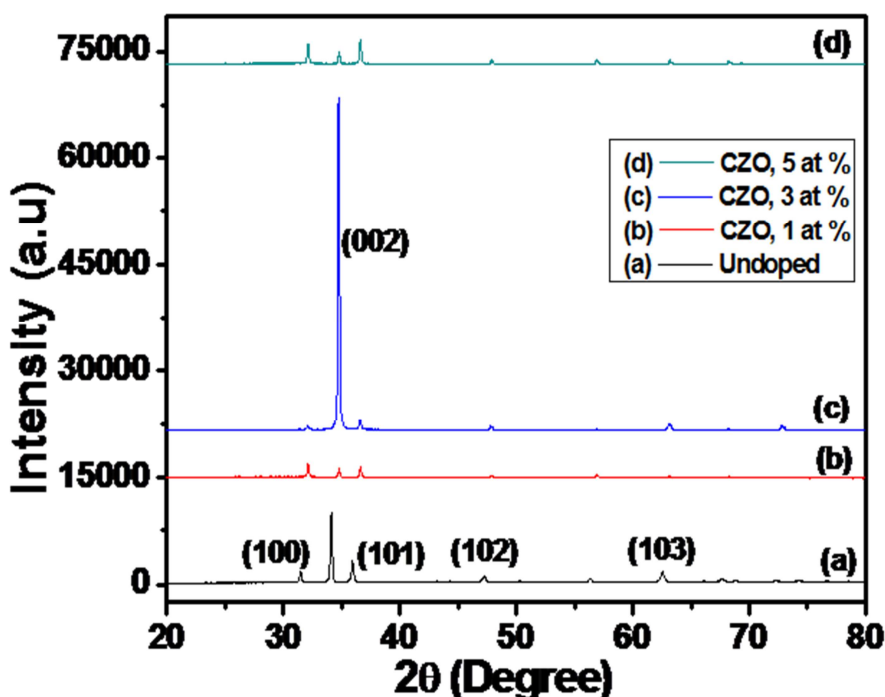
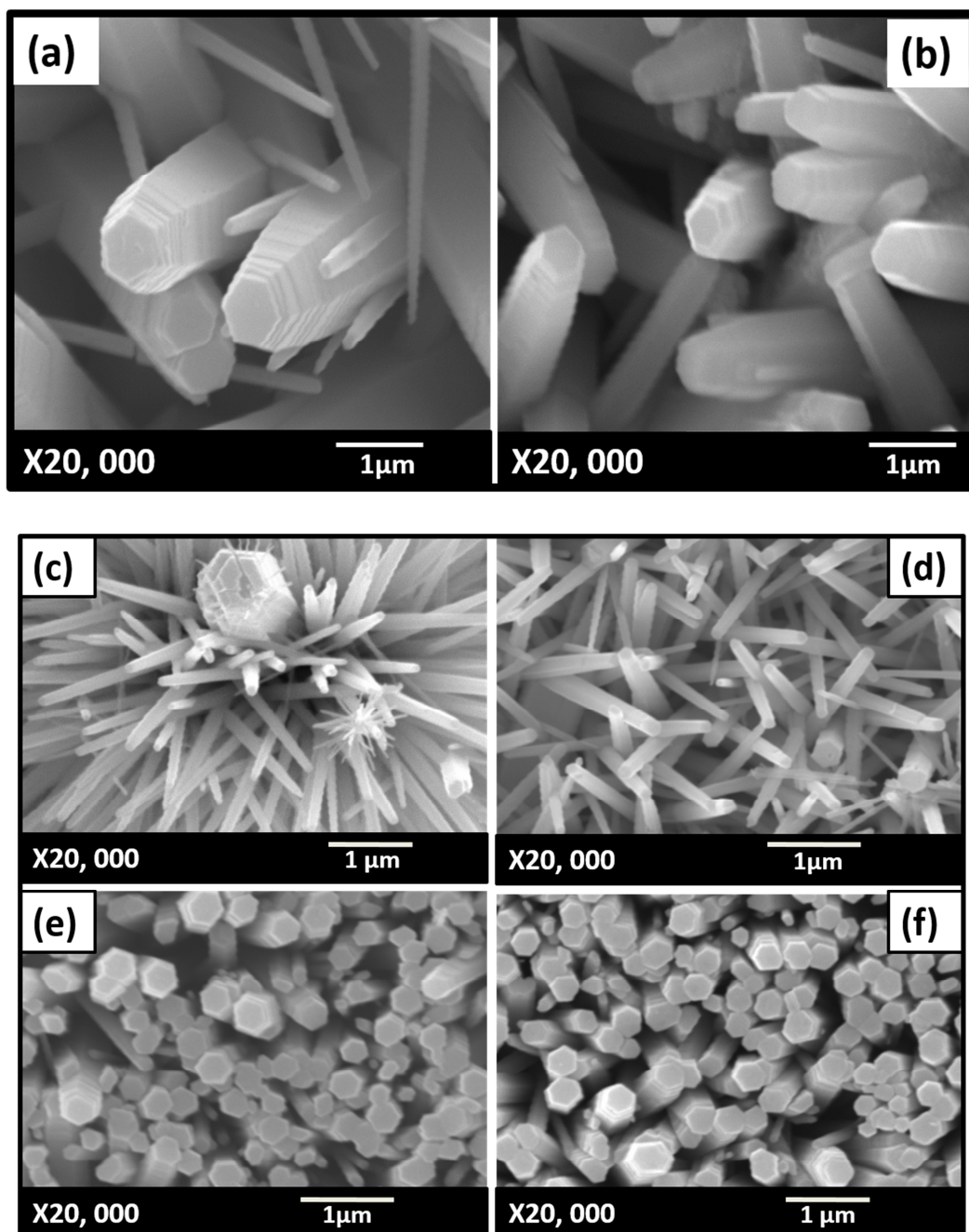


Fig. 1. XRD micrographs of CZO with different Cu dopings: (a) undopedZnO (b) 1 at % (c) 3 at % and (d) 5 at %

Fig. 6a-c, depicts the impedance spectra of *indigofera arrecta* plant dye-sensitized CZO PEC solar cells with different Cu concentrations (1, 3 and 5 at. %) measured in the dark at various applied voltages (0.656, 0.844 and 0.790 V). Fig. 6 a(iii) and c(iii) indicate that the PEC cells of CZO for Cu:ZnO of 1 and 5 at. % have similar circuit models; in fact, it is a transmission line model [48, 50]. In the model, R_s , the series resistance, which includes the sheet resistance of the stainless steel and the external contact resistance of the cell (e.g. wire connections), is negligible. The parallel R_1 (ohmic resistance) and C_μ (represented by constant phase elements, CPE, Q_1) elements characterize the charge transfer resistance and the double layer capacitance, Q_2 in the semiconductor, respectively [47, 48]. The Nyquist plots, Fig. 6 a(i) and c(i) (for Cu:ZnO of 1 and 5 at. %) indicates a relatively moderate overall cell impedance which showed an exponential decay over the entire frequency range of measurement (aii and cii) however, the observed impedance values are much lower for Cu:Zn of 5 at. %. The impedance is observed to decrease rapidly from Cu:ZnO of 1 at. % to a minimum at 3 at.% doping concentration and there after increases again.

Under the measured condition (ie; in the dark), the charge-transfer resistance in the semiconductor and the diffusion within the electrolyte are represented by $R_1//Q_1$ (aiii and ciii) and is lower for *indigofera arrecta* plant dye-sensitized CZO electrodes with Cu content of 5 at. %. This implies better PEC performance. Fig. 6 a(ii) and c(ii) (curve b in

each case), shows single time constants denoted by the high frequency peaks in the Bode-Phase diagrams which correspond to the diffusion within the electrolyte and the electron transport/recombination process in the semiconductor [51, 52]. In both cases, the charge transport impedance at the mesoporous oxide layer contributed by the series resistance in the high frequency range of the Nyquist plots (ai, iii and ci, iii) is low since the series resistance of the oxide layer in these cases is zero. The Bode plots a(ii) and c(ii) (curve a) show similar results.



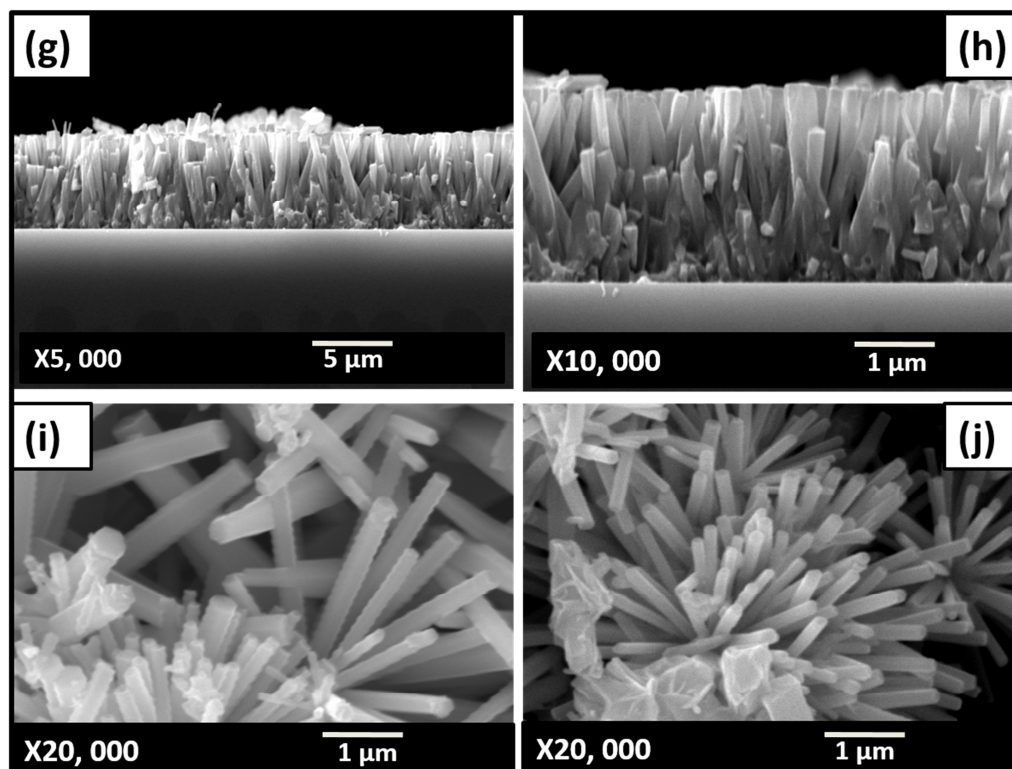


Fig. 2. SEM micrographs of CZO thin films with different Cu dopings (a, b) 1 at %, as-deposited and annealed (c, d) 3 at %, as-deposited and annealed (e, f) cross-sectional view of (d) (g, h) 5 at %, as-deposited and annealed

Fig. 6b, represents the impedance spectra of the PEC solar cell of CZO electrode for 3 at. % doping level. Similarly (to 1 and 5 at %), the series resistance of the cell is zero (biii) and the cell impedance is minimum for this doping concentration (bi) which implies maximum PEC solar cell performance as seen in Table 2. The transmission line model is also employed here to determine the cell impedance [48, 50, 57]; the parallel R_1 and C_1 elements characterize the charge transfer resistance and the double layer capacitance in the semiconductor are clearly represented, thus the diffusion of charge carriers at the semiconductor/electrolyte interface can now be represented by an R/C -circuit element [51, 52]. In a similar way, the platinized counter-electrode is characterized by a charge-transfer resistance, R_2 , and a double layer capacitance, C_2 [51, 52, 57]. In the dark, the diffusion of Zn^{2+} within the electrolyte solution is represented by a Warburg element, W as depicted in Fig. 6 b(iii) [53-57]. In fact, a very good agreement between experimental and fitted data was obtained as in b(i). The estimated values of the cells impedance elements derived from the electrical analogs, are presented in Table 3 (a, b and c), and were used to fit the EIS experimental data in the two-electrode configuration in dark condition.

4.3. Power Conversion Efficiency (η) and Fill Factor (FF)

Energy or power conversion efficiency (η) of solar cell is the percentage of power converted from the absorbed light to electrical energy and collected, when a solar cell is connected to an electrical circuit. The power outputs of the dye-sensitized CZO thin film PEC solar cells in the current work were determined in the dark and under illumination with an input power (P_{in}), of 80 mW/cm^2 .

All the currents and potentials (I_{sc} , V_{oc} , I_{max} and V_{max}) measured for the CZO thin film electrodes sensitized with *indigofera arrecta* plant dye are shown in the I-V curve of Fig. 5 and the measured values are presented in Table 2, respectively. The light energy to electrical power conversion efficiency (η) and fill factor (FF) were evaluated from the following Eqns:

$$\eta(\%) = \frac{I_{max} (A/cm^2) V_{max} (V)}{P_{in} (W/cm^2)} \times 100 \quad (6)$$

$$FF = \frac{I_{\max} (A/cm^2) V_{\max} (V)}{I_{sc} (A/cm^2) V_{oc} (V)} \quad (7)$$

The estimated values of power conversion efficiencies and fill factors for all the CZO thin film electrodes are presented in Table 4.

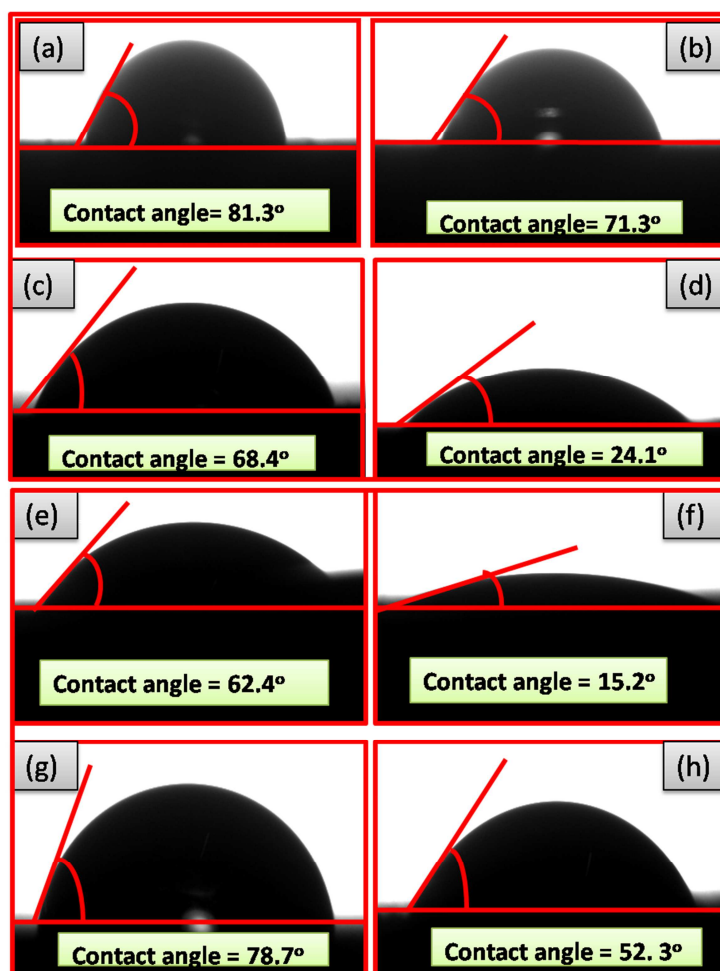


Fig. 3. Water contact angle measurement of (a, b) undoped ZnO, as-deposited and annealed (c, d) CZO thin films 1 at %, deposited and annealed (e, f) CZO thin films 3 at %, deposited and annealed and (g, h) CZO thin films 5 at %, deposited and annealed

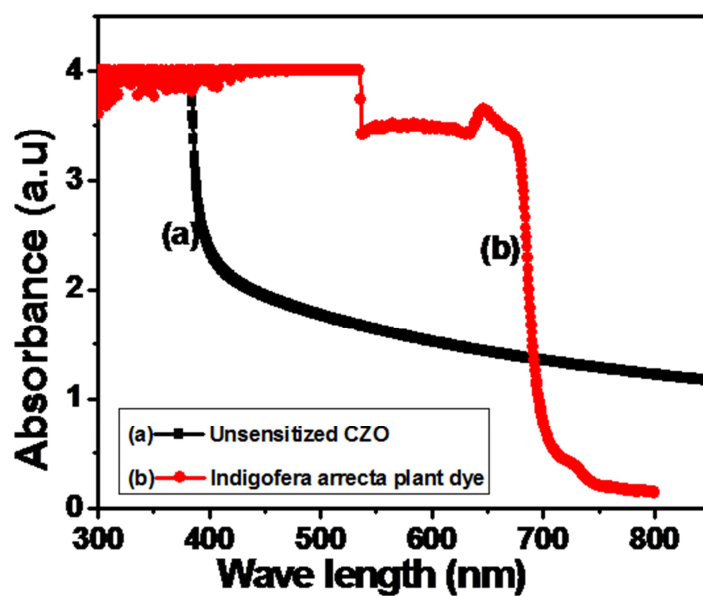
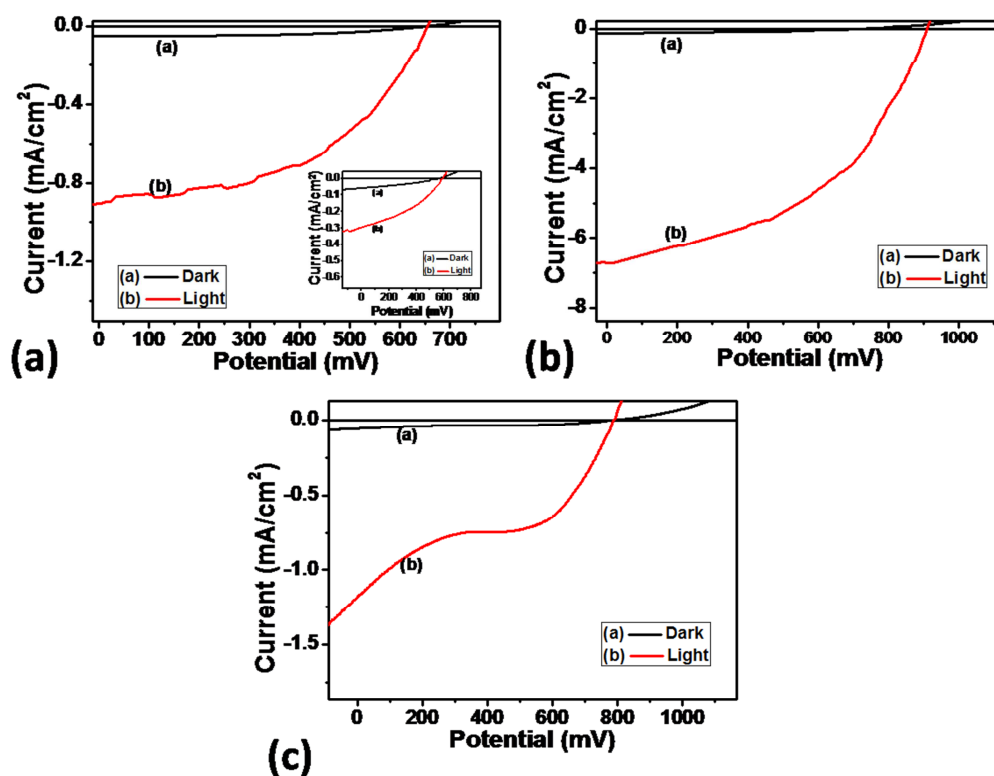
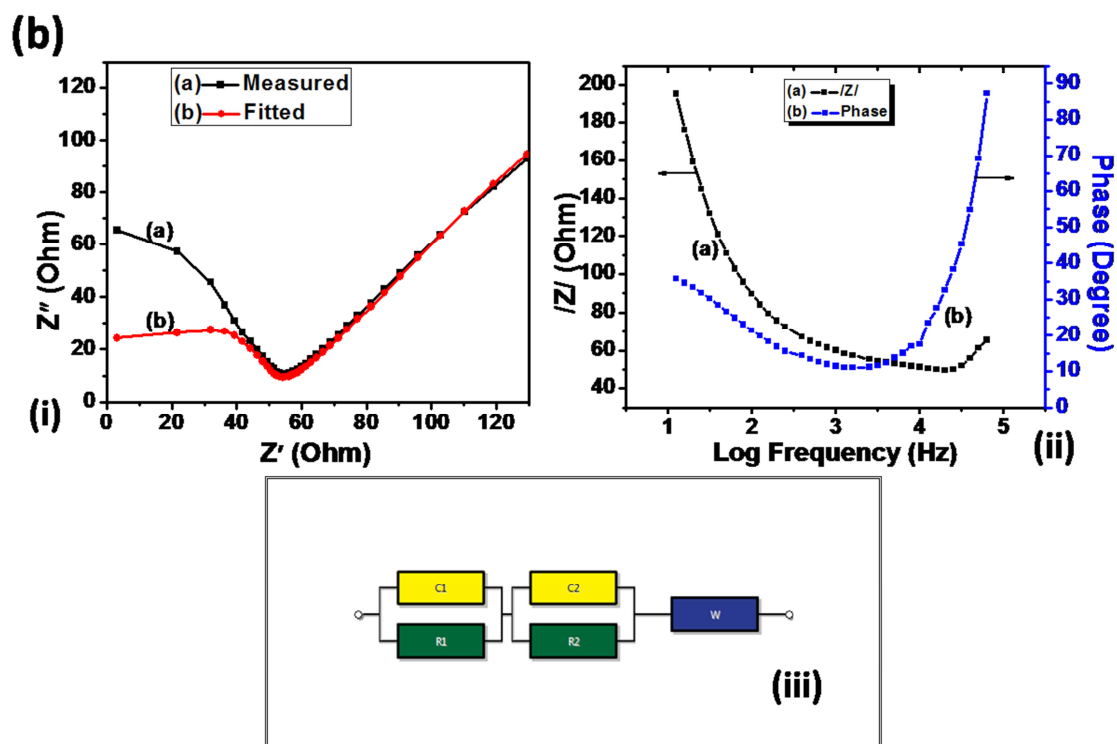
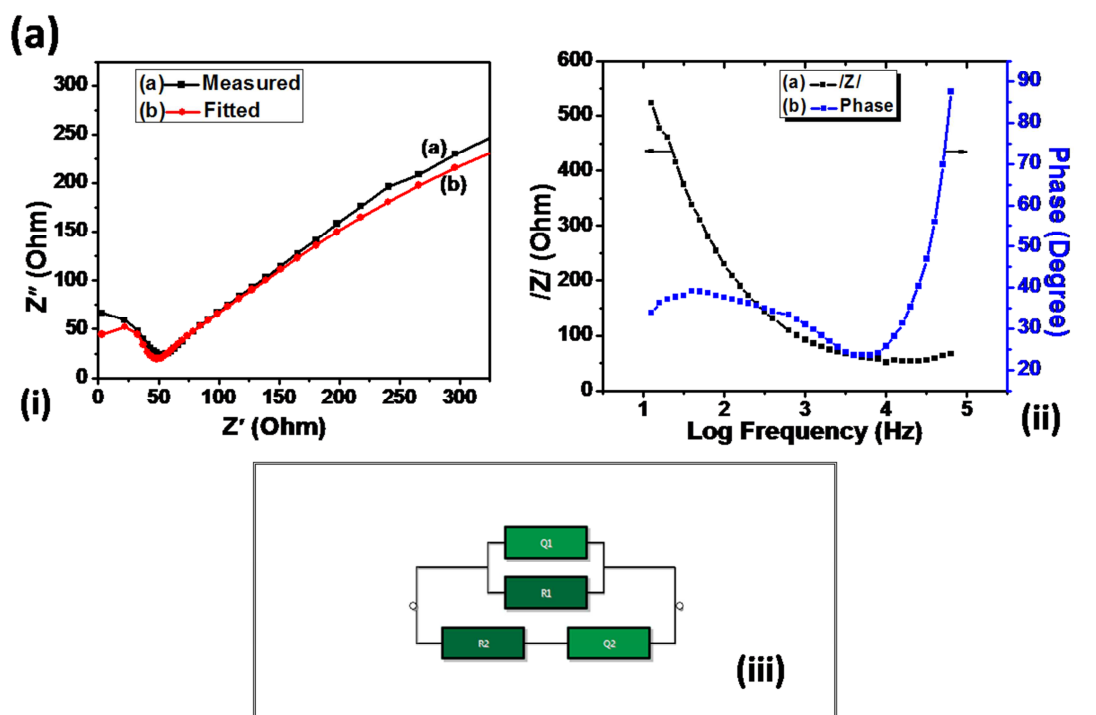
Fig. 4. Absorption spectrum of *Indigofera arrecta* plant dye in acetonitrile

Fig. 5. Current-potential curves for dye-sensitized nanocrystalline CZO electrodes with different Cu dopings (a) 1 at % (b) 3 at % and (c) 5 at %



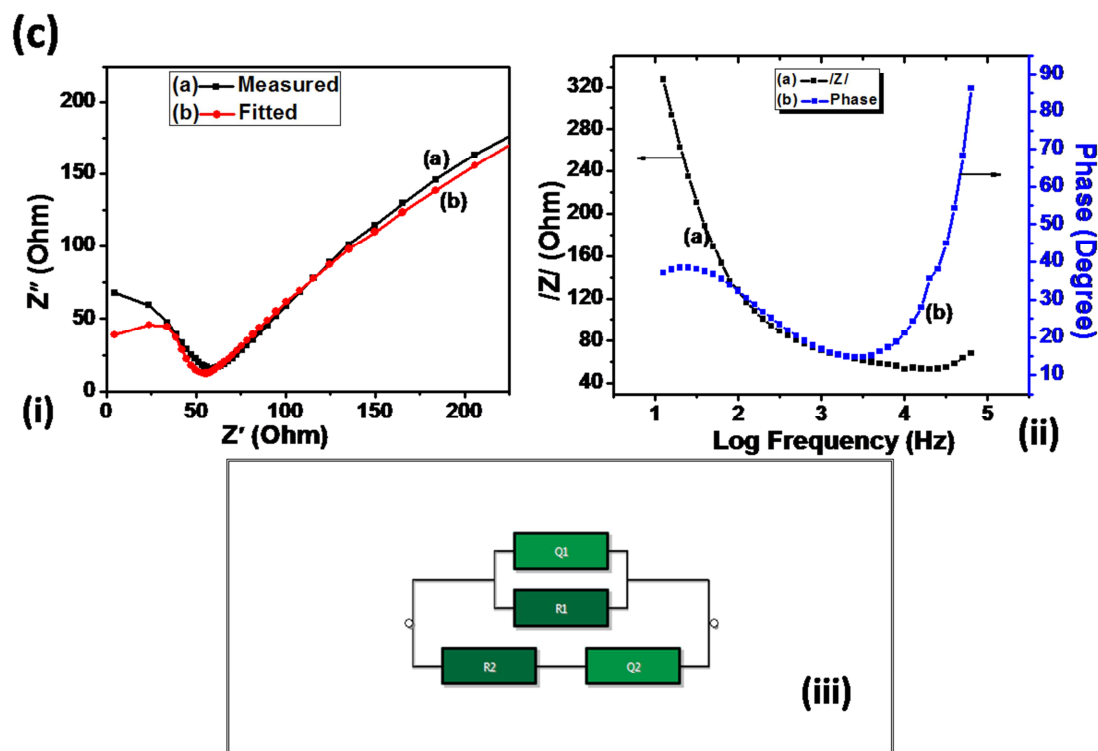


Fig. 6. Impedance spectra of *indigofera arrecta* plant dye-sensitized CZO PEC solar cell with different Cu dopings: (a) 1 at % (b) 3 at % (c) 5 at % obtained in dark at bias potentials of 0.656, 0.914 and 0.790 V

CONCLUSION

PEC solar cell characterization of CZO thin film electrodes sensitized by a natural dye obtained from *indigofera arrecta* plant has been successfully carried out. The study has shown that, the synthesized CZO thin film electrodes has porous nanostructures, were strongly hydrophilic and indicated red shifts in their absorption spectra up to 450 nm wavelength. Further with the use of *indigofera arrecta* plant dye on CZO electrode, the spectral response of the wide band gap CZO (3.14 eV, optimal) was extended well into the visible region up to 750 nm wavelength. *Indigofera arrecta* plant dye was seen to anchor well on nanocrystalline CZO thin film electrode. The use of the dye on CZO electrode shows significant enhancement in PEC cell properties of the semiconductor. Photocurrent and photovoltage of 6.8 mA/cm² and 0.844 V were measured which yielded light to electrical energy and fill factor of 4.16 % and 0.54, respectively. EIS study of the PEC solar cells also confirms good performance. It is obvious from this study that CZO semiconductor materials sensitized with *Indigofera arrecta* plant dye are better candidates for PEC solar cells application than undoped ZnO.

REFERENCES

- [1] Srivastava P, Bahadur L, *Inter. J. Hydrog. Ener.*, **2012**, 37, 4863.
- [2] Hardin B E, Snaith H J, McGehee M D, *Nature Photonics*, **2012**, 6, 162.
- [3] Kuang D, Ito S, Wenger B, Klein C, Moser J E, Humphry-Baker R, Zakeeruddin S M, Grätzel M, *J. Am. Chem. Soc.*, **2006**, 128, 4146.
- [4] Grätzel M, *Nature*, **2001**, 414, 338.
- [5] Sekar N, Gehlot V Y, *Resonance*, **2010**, 819.
- [6] Argazzi R, Larramona G, Contado C, Bignozzi C A, *J. Photochem. Photobiol. A*, **2004**, 164, 15.
- [7] Nazeeruddin M K, Wang Q, Cevey L, Aranyos V, Liska P, Figgemeier E, Klein C, Hirata N, Koops S, Haque S A, Durrant J R, Hagfeldt A, Lever A B P, Grätzel M, *Inorgan. Chem.*, **2006**, 45, 787.
- [8] Mayo E, Kilsa K, Tirrell T, Djurovich P I, Tamayo A, Thompson M E, *Photochem Photobiol. Sc.*, **2006**, 5, 871.
- [9] Grätzel M, *J. Photochem. Photobiol. A*, **2004**, 164, 3.

- [10] Chen C, Wang M, Li J, Pootrakulchote N, Alibabaei L, Ngocle C, *ACS Nano*, **2009**, 3, 3103.
- [11] Jiang K J, Masaki N, Xia J B, Noda S, Yanagida S, *Chem. Commun*, **2006**, 23, 2460.
- [12] Ito S, Matsui H, Okada K, Kusano S, Kitamura T, Wada Y, Yanagida S, *Sol. Ener. Mater. Sol. Cells*, **2004**, 82, 421.
- [13] Souad A M, Al-Bat'hi, Alaei I, Sopyan I, *Inter. J. Renew. Ener. Res.*, **2013**, 3, 138.
- [14] Raidou A, Aggour M, Qachaou A, Laana L, Fahoume M, *M. J. Conden. Matter*, **2010**, 12, 125.
- [15] Taya S A, El-Agez T M, El-Ghamri H S, Abdel-Latif M S, *Inter. J. Mater. Sc. Appl.*, **2013**, 2, 37.
- [16] Chu S, Li D, Chang P C, Lu J G, *Nanoscale Res Lett*, **2011**, 6, 38.
- [17] G. Zhang, H. Bala, Y. Cheng, D. Shi, X. Lv, Q. Yu, P. Wang, *Chem. Commun.* **2009**, 2198.
- [18] Roy M S, Balraju P, Kumar M, Sharma G D, *Sol. Energ. Mater. Sol. Cells*, **2008**, 92, 909.
- [19] Hara K, Tachibana Y, Ohga Y, Shinpo A, Suga S, Sayama K, Sugihara H, Arakawa H, *Sol. Ener. Mater. Sol. Cells*, **2003**, 77, 89.
- [20] Sarto Polo A, Murakami Iha N Y, Itokazu M K, *Coord. Chem. Rev.*, **2004**, 248, 1343.
- [21] Fernando J M R C, Sendeera G K R, *Res. Comm. Curr. Sci.*, **2008**, 95, 663.
- [22] Hao Y, Yang M, Li W, Qiao X, Zhang L, Cai S, *Sol. Ener. Mater. Sol. Cells*, **2000**, 60, 349.
- [23] Mishra A, Markus K, Fischer R, Bäuerle P, *Angew. Chem. Int. Ed.* **2009**, 48, 2474.
- [24] Bahadur L, Srivastava P, *Sol. Ener. Mater. Sol. Cells*, **2003**, 79, 235.
- [25] Chow L, Lupan O, Chai G, Khallaf H, Ono L K, Roldan K, Cuenya B, Tiginyanu I M, Ursak V V, Sontev, Schulte A, *Sensors and Actuators A*, **2013**, 189, 399.
- [26] Shinde V R, Lokhande C D, Mane R S, Han Sung-Hwan, *Appl. Surf. Sc.*, **2005**, 245, 407.
- [27] Drici A, Djeteli G, Tchangbedgi G, Deruiche H, Jondo K, Napo K, Barnede J C, Ouro-Djobom S, Gbagba M, *Phys. Stat. Sol. (a)*, **2004**, 201, 1528.
- [28] Gondoni P, Mazzolini P, Russo V, Petrozza A, Srivastava A K, Bassia AL, Casaria C S, *Sol. Ener. Mater. Sol. Cells*, **2014**, 128, 248.
- [29] Chauhan R, Kumar A, Chaudhary R P, *J. Chem. Pharm. Res.* **2010**, 2, 178.
- [30] Yao PC, Hang ST, Lin YS, Yen WT, Lin Y C, *Appl. Surf. Sc.*, **2010**, 257, 1441.
- [31] Kim J, Shin H, *J. Phys. Chem. C*, **2010**, 114, 7185.
- [32] Herng T S, Lau S P, Yu S F, Yang H Y, Wang L, Tanemura M, Chen J S, *Appl. Phys. Lett.* **2007**, 90, 032509.
- [33] Lupan O, Pauporte T, Le Bahers T, Viana B, Ciofini I, *Ad. Funct. Mater.* **2011**, 21, 3564.
- [34] Shannon R D, *Acta Crystallograph. Sect. A, Cryst. Phys., Diffract. Theoret. Gener. Crystallography* **1976**, 32, 751.
- [35] Kulkarni S B, Patil U M, Salunkhe R R, Joshi S S, Lokhande C D, *J. Alloys and Compounds*, **2011**, 509, 3486.
- [36] Kakiuchi K, Saito M, Fujihara S, *Thin Solid Films*, **2008**, 516, 2026.
- [37] Shrestha S P, Ghimire R, Nakarmi J J, Kim Y S, Shrestha S, Park C Y, Boo J H, *Bull. Korean Chem. Soc.*, **2010**, 31, 112.
- [38] Zhou Z, Kato K, Komaki T, Yoshino M, Yukawa H, Morinaga M, Morita K, *J. Electroceram.* **2003**, 11, 73.
- [39] Sun R D, Nakajima A, Fujishima A, Watanabe T, Hashimoto K, *J. Phys. Chem. B*, **2001**, 105, 1984.
- [40] Sun H, Luo M, Weng W, Cheng K, Du P, Shen G, Han G, *Nanotechnol.* **2008**, 19, 125603.
- [41] Bhattacharya C, Datta J, *Mater. Chem. Phys.*, **2005**, 89, 170.
- [42] Nogami M, Suwa M, Kasuga T, *Solid State Ionics*, **2004**, 166, 39.
- [43] Kim J D, Honma I, *Electrochim. Acta*, **2004**, 49, 3179.
- [44] Rekha D, Lijin R B, Hyun G K, Pramod H B, *Inter. J. Photoener.* **2013**, 928321.
- [45] Hsu C H, Chen D. H, *Nanoscale Res. Lett.*, **2012**, 7, 593.
- [46] Sekar N, Ramasamy R P, *J. Microbial Biochem Technol*, **2013**, S6.
- [47] Rodríguez E G, A Ph.D Thesis in Department of Physical, Chemical and Natural systems, *University Pablo de Olavide* **2011**, 59.
- [48] Patil S B, Singh A K, *Electrochim. Acta* **2011**, 56, 5693.
- [49] Bisquert V, Vikhrenko V S, *J. Phys. Chem. B*, **2004**, 108, 2313.
- [50] Lopes T, Andrade L, Ribeiro H A, Mendes A, *Int. J. Hydrog. Ener.* **2010**, 35, 11601.
- [51] Lagemaat J V D, Frank A J, *J. Phys. Chem. B*, **2001**, 105, 11194.
- [52] Bisquert J, Mara-Seró I, *J. Phys. Chem. Lett.*, **2010**, 1, 450.
- [53] Jennings J R, Ghicov A, Peter L M, Schmuki P, Walker A B, *J. Amer. Chem. Soc.* **2008**, 130, 13364.
- [54] Boudjema A, Boumaz S, Trari M, Bouguelia A, *Inter. J. Hydrog. Ener.* **2009**, 34, 4268.
- [55] Gabás M, Barrett N T, Ramos-Barrado J R, Gota S, Rojas T C, López-Escalante M C, *Sol. Ener. Mater. Sol. Cells*, **2009**, 93, 356.
- [56] Haqa BU, Ahmed R, Goumri-Said S, *Sol. Ener. Mater. Sol. Cells*, **2014**, 130, 6.
- [57] Sunga Y M, Hsu F C, Chen Y F, *Sol. Ener. Mater. Sol. Cells*, **2014**, 125, 239.